Research Square

Preprints are preliminary reports that have not undergone peer review.
They should not be considered conclusive, used to inform clinical practice,
or referenced by the media as validated information.

Bioinformatics and In Vivo Experiments Identify Hmgcs2 as a Key Gene Linking Fatty Acid Metabolism and Lactylation in Acute Kidney Injury Associated with Sepsis

Jinzhi Song
Shanxi Medical University
Yawen Wu
Shanxi Medical University
Gehui Xiao
Shanxi Medical University
Xueqin Li
Shanxi Medical University
Hongmei Zhang
Shanxi Medical University
Na Xia
Shanxi Medical University
Jianying Bai
Shanxi Medical University
Xuan Shang
shangxuan@sxmu.edu.cn
Shanxi Medical University

Research Article

Keywords: Sepsis-associated acute kidney injury, Hmgcs2, Fatty acid metabolism, Lactylation, Bioinformatics, Machine learning

Posted Date: November 12th, 2026

DOI: https://doi.org/10.21203/rs.3.rs-11306189/v1

License: This work is licensed under a Creative Commons Attribution 4.0 International License.
Read Full License

Additional Declarations: No competing interests reported.

Bioinformatics and *In Vivo* Experiments Identify Hmgcs2 as a Key Gene Linking Fatty Acid Metabolism and Lactylation in Acute Kidney Injury Associated with Sepsis

Jinzhi Song[1,3,#], Yawen Wu[1,2,#], Gehui Xiao[1,2], Xueqin Li[1,4], Hongmei Zhang[3], Na Xia[3,*], Jianying Bai[3,*], Xuan Shang[1,4,*]

[1] Key Laboratory of Cellular Physiology, Ministry of Education, Shanxi Medical University, Taiyuan, 030001, China

[2] Second Clinical Medical College, Shanxi Medical University, Taiyuan 030001, China

[3] School of Public Health, Shanxi Medical University, Taiyuan 030001, China

[4] Department of Physiology, Shanxi Medical University, Taiyuan 030001, China

[#] These authors contributed equally to this work

[*]Corresponding authors

Na Xia: xiana528@163.com

Jianying Bai: jybai66@sxmu.com.cn

Xuan Shang: shangxuan@sxmu.edu.cn

Abstract

Background: Sepsis-associated acute kidney injury (S-AKI) is a severe critical care complication with high morbidity and mortality, involving inflammatory dysregulation, metabolic reprogramming, and immune dysfunction. However, the molecular link between fatty acid metabolism disorders and lactylation in S-AKI remains unclear, and systematic screening with functional validation is lacking.

Methods: Based on mouse kidney transcriptome datasets, we performed DEGs analysis, GSEA, GO/KEGG enrichment, and LASSO regression to screen key candidates. Intersection analyses with fatty acid metabolism and lactylation-related gene sets were conducted to identify core targets. Diagnostic value was evaluated by ROC curves, immune infiltration by CIBERSORT, and *in vivo* validation in a CLP-induced S-AKI mouse model.

Results: A total of 359 DEGs were identified, with GSEA revealing significant enrichment of inflammation and metabolism pathways. LASSO narrowed candidates to 16 feature genes. Four-set Venn intersection identified Hmgcs2 as the only core target

intersecting both fatty acid metabolism and lactylation-related gene sets. ROC analysis confirmed good diagnostic efficacy (AUC > 0.7). Immune infiltration showed increased M0 macrophages and neutrophils in S-AKI, significantly correlated with Hmgcs2 expression. *In vivo* experiments confirmed significant upregulation of Hmgcs2 mRNA and protein in renal tissues after CLP.

Conclusion: This study, integrating bioinformatics, machine learning, and in vivo experiments, incorporates fatty acid metabolism and lactylation into a unified screening framework and identifies Hmgcs2 as a key network node bridging these two dimensions. As the rate-limiting enzyme of ketogenesis, Hmgcs2 may regulate renal energy homeostasis through FAO and potentially influence lactylation-related epigenetic networks by reshaping the metabolic microenvironment, exerting renoprotective effects in S-AKI. Hmgcs2 shows promise as a diagnostic biomarker and therapeutic target for S-AKI.

Keywords: Sepsis-associated acute kidney injury; Hmgcs2; Fatty acid metabolism; Lactylation; Bioinformatics; Machine learning

1 Introduction

Sepsis is a systemic inflammatory response syndrome caused by infection and represents one of the leading causes of death among patients in intensive care units (ICUs)[1]. Sepsis-associated acute kidney injury (S-AKI) is the most common serious complication of sepsis, occurring in approximately 45–70% of septic patients, and significantly increases mortality risk and prolongs hospital stay[2,3]. The clinical features of S-AKI include elevated serum creatinine, reduced urine output, and decreased glomerular filtration rate[3]. Although understanding of S-AKI has deepened in recent years, its pathogenesis remains incompletely elucidated, and effective targeted therapeutic interventions are still lacking.

The pathophysiological mechanisms of S-AKI are extremely complex, involving interactions among multiple processes such as aberrant immune responses, microcirculatory dysfunction, mitochondrial dysfunction, metabolic reprogramming, and cell death[4]. Among these, the critical role of metabolic disturbances in the pathogenesis of S-AKI has received increasing attention[5–7]. Under normal physiological conditions, renal proximal tubular epithelial cells (TECs) primarily rely on mitochondrial fatty acid β-oxidation (FAO) as an energy source[8,9]. However, under septic conditions, FAO is suppressed, and glycolysis is compensatorily enhanced, leading to mitochondrial dysfunction, lipid accumulation, and aggravated tubular

injury[10,11]. Metabolomic studies have likewise confirmed that mitochondrial-related pathways, including FAO, branched-chain amino acid metabolism, and NAD^+ synthesis, are significantly inhibited in S-AKI[12]. PPARα, a key transcriptional regulator of fatty acid metabolism, exerts important protective effects in septic AKI, and PPARα-deficient mice exhibit worsened renal function, closely associated with reduced FAO and enhanced inflammation[13]. Fenofibrate, a clinically available PPARα agonist, has been shown to attenuate S-AKI by enhancing renal FAO and mitochondrial energy metabolism via the AMPK–PGC1α–PPARα pathway[3]. The above evidence strongly suggests that FAO and its upstream regulatory network may represent critical protective pathways in S-AKI, but the specific molecules that play core roles within this network remain to be systematically identified.

Concurrently, the role of protein post-translational modifications in the metabolic regulation of S-AKI has emerged as a research hotspot[14]. Lactylation, as a novel protein post-translational modification, has attracted extensive attention in S-AKI research in recent years. Lactate has long been regarded as a metabolic waste product of glycolysis and a marker of tissue hypoperfusion, but recent studies have revealed that lactate can function as a signaling molecule through protein lactylation[15,16]. Under septic conditions, increased systemic lactate production, impaired lactate clearance, and renal metabolic reprogramming collectively contribute to lactate accumulation[17]. A large-scale clinical study based on the MIMIC-IV database, encompassing 11,431 septic patients, confirmed that high lactate levels are independently associated with an increased risk of S-AKI, whereas higher lactate clearance rates correlate with better renal outcomes[15]. In septic mouse models, kidney-specific protein lactylation is significantly upregulated, whereas this phenomenon is not observed in the heart, liver, or spleen, suggesting a potential molecular link between lactate metabolism and renal susceptibility[15]. Mechanistically, lactylation can influence chromatin structural remodeling and gene expression regulation through lysine lactylation of histones and non-histone proteins[15]. For example, lactate-induced HMGB1 lactylation in macrophages promotes neutrophil extracellular trap formation and exacerbates AKI via the cGAS/STING pathway[15]; histone H3K18 lactylation-mediated SPHK1-SIRT1 feedback loop accelerates TEC pyroptosis[18]. These findings indicate that lactylation plays an important pathological regulatory role in S-AKI, but which key molecules are regulated by lactylation remains unclear.

Notably, fatty acid metabolism and lactylation are not mutually independent biological

processes; acetyl-CoA generated from fatty acid β-oxidation is not only a core intermediate product of energy metabolism but also indirectly regulates the availability of upstream substrates for various acylation modifications, including lactylation, by influencing the composition and abundance of the acyl-CoA pool[19–21]. However, to date, no study has systematically screened for common key molecules that are simultaneously involved in the regulation of fatty acid metabolism and the lactylation modification network at the systemic level. In S-AKI, does there exist one or several genes that are not only closely related to fatty acid metabolism but also potentially indirectly influence lactylation through the metabolite network? This scientific question remains unanswered, and the key to addressing this question lies in unbiased, genome-wide screening of core nodes that are simultaneously associated with both of the aforementioned biological processes.

In recent years, the rapid development of bioinformatics and machine learning methods has provided powerful tools for efficiently screening key molecules from transcriptomic databases of complex diseases[22]. Differential expression gene (DEG) analysis combined with gene set enrichment analysis (GSEA) can systematically identify disease-related pathways; machine learning algorithms such as LASSO can select the most characteristic key genes from high-dimensional data; and multi-gene-set intersection analysis can focus the screening scope onto specific biological processes[23,24]. Based on this, the present study proposes the following research strategy: using the transcriptomic data of kidney tissues from S-AKI mice as a starting point, DEGs were identified and feature genes were screened via the LASSO algorithm, and then subjected to intersection analysis with fatty acid metabolism-related gene sets and lactate metabolism-related gene sets, respectively, thereby identifying core target genes that simultaneously connect the two biological processes. Notably, since lactate is the direct substrate source for lactylation modification, screening for lactate metabolism-related gene sets can effectively identify key molecules that may influence the lactylation modification network by altering lactate levels. On this basis, the diagnostic value of candidate genes is evaluated by ROC curves, and their association with the renal immune microenvironment is explored through immune infiltration analysis. Finally, this study further constructs a CLP-induced S-AKI mouse model for in vivo validation. The present study aims to systematically screen and validate key protective genes in S-AKI from the novel perspective of the interplay between fatty acid metabolism and lactylation modification, with the goal of providing new theoretical foundations and potential targets for mechanistic research and clinical

translation in S-AKI.

2 Materials and Methods

2.1 Data Sources and Preprocessing

The S-AKI gene expression data utilized in this study were derived from the GSE60088 and GSE225192 datasets in the Gene Expression Omnibus (GEO) database (https://www.ncbi.nlm.nih.gov/geo). These two datasets collectively comprised renal tissue transcriptomic sequencing data from 135 S-AKI mouse model cases and 32 corresponding control cases (GSE60088: CONTROL—12, TREAT—15; GSE225192: CONTROL—20, TREAT—120; total: CONTROL—32, TREAT—135). Raw data were normalized using the Robust Multi-array Average (RMA) algorithm to mitigate batch effects and systematic errors. Quality control metrics for all samples met the requirements for subsequent analyses. The lactate metabolism-related gene set was sourced from the MsigDB database. Fatty acid metabolism-related gene lists were obtained from the Genecard database.

2.2 Screening of Differentially Expressed Genes (DEGs)

Differential expression analysis between the S-AKI and control groups was performed using the "limma" package in R 4.2.0. Specifically, raw CEL files were first subjected to background correction, quantile normalization, and probe summarization using the RMA algorithm from the affy package; data from the Illumina platform were normalized using variance-stabilizing transformation (VST) from the lumi package. Outlier samples were removed via hierarchical clustering. Probe IDs were converted to official gene symbols, and for genes with multiple probes, the mean expression value was calculated. To eliminate batch effects across datasets, the ComBat function (sva package) was applied with dataset origin as the batch variable, yielding a batch-corrected normalized expression matrix. Genes without gene symbols and those with median expression values < 1 were excluded. DEGs were screened using the Limma package with thresholds of $|\log2FC| > 1$ and adjusted $P < 0.05$. Differential expression analysis was performed using the limma package, with adj.$P < 0.05$ set as the significance threshold. Additionally, DEGs were visualized using volcano plots and heatmaps. Volcano plots were generated using the "ggplot2" package, with log2FC on the x-axis and -log10(adj.*P*.Val) on the y-axis; red indicated upregulated genes and blue indicated downregulated genes. Heatmaps were generated using the "pheatmap" package to display the expression clustering patterns of the top 60 DEGs between the two groups.

2.3 Gene Set Enrichment Analysis (GSEA)

GSEA was performed on the entire gene set ranked by log2FC to capture coordinated pathway perturbations. To comprehensively capture coordinated pathway perturbations at the genome-wide level, Gene Set Enrichment Analysis (GSEA) was performed on all genes ranked by expression differences. Specifically, genes were first ranked by log2FC values to generate .rnk format ranking files. The hallmark gene sets (h.all.v7.5.1.symbols.gmt) and KEGG pathway gene sets (c2.cp.kegg.v7.5.1.symbols.gmt) from the Molecular Signatures Database (MSigDB, https://www.gsea-msigdb.org/gsea/msigdb) were used as reference gene sets. GSEA was performed using the clusterProfiler package in R 4.5.0. The Normalized Enrichment Score (NES) and False Discovery Rate (FDR) were used to assess the significance of pathway enrichment. The significance thresholds for enrichment were FDR < 0.25 and $P < 0.05$.

2.4 Protein-Protein Interaction (PPI) Network Analysis

PPI network analysis helps reveal functional connections among proteins and identify key nodes within the network, which typically play central regulatory roles in biological processes. DEGs were imported into the STRING database (https://string-db.org/) for PPI network analysis, with the species set to "Mus musculus" and the minimum interaction score set to ≥ 0.5. After exporting the interaction data in TSV format, the PPI network was visualized using Cytoscape software V 3.10.3. Network topology analysis was performed using its built-in NetworkAnalyzer tool, which calculated topological parameters including Closeness Centrality, Betweenness Centrality, and Degree for each node. Core target genes with Degree > 1 were screened based on Degree ranking.

2.5 Functional Enrichment Analysis

GO functional annotation helps systematically elucidate the biological functions involving the core targets, while KEGG pathway enrichment analysis can reveal the signaling transduction and metabolic pathways regulated by the core targets. The combination of these analyses provides an important basis for understanding the potential molecular mechanisms underlying the association of 6PPD-Q with breast cancer. Specifically, GO analysis encompasses three dimensions: biological process (BP), cellular component (CC), and molecular function (MF). In this study, GO and KEGG enrichment analyses were performed using the clusterProfiler package, with the significance threshold set at adjusted $P < 0.05$.

2.6 LASSO Regression Analysis

The Least Absolute Shrinkage and Selection Operator (LASSO) regression algorithm was employed for further screening of candidate genes. LASSO regression analysis was performed using the glmnet package in R software. Specifically, the DEG expression matrix was used as feature variables, and sample grouping (S-AKI vs. control) served as the response variable. Ten-fold cross-validation was performed using the cv.glmnet function to select the optimal penalty parameter λ that minimized the cross-validation deviance (cv.glmnet: family = "binomial", alpha = 1, type.measure = "deviance", nfolds = 10). The LASSO model was then fitted using the glmnet function with the optimal λ value. Genes with non-zero coefficients were extracted as core genes selected by LASSO.

2.7 Identification of Core Targets

Four gene sets—DEGs, LASSO-selected genes, lactate metabolism-related genes, and fatty acid metabolism pathway-related genes—were subjected to Venn diagram intersection analysis. The resulting overlapping genes were identified as the core targets of S-AKI.

2.8 ROC Analysis

Receiver Operating Characteristic (ROC) curve analysis was performed on the final identified core genes to evaluate their diagnostic value for S-AKI. ROC analysis was conducted using the pROC package in R software. First, core gene expression values were used as predictor variables, and sample grouping served as the outcome variable. ROC curves were calculated using the roc function, and the Area Under the Curve (AUC) with 95% confidence intervals was calculated using the auc function. The optimal cutoff values with corresponding sensitivity and specificity were determined using the ci.thresholds function. An AUC > 0.7 was considered to indicate moderate diagnostic value, while an AUC > 0.9 indicated high diagnostic value.

2.9 Immune Infiltration Analysis

Immune cell infiltration analysis of renal tissue transcriptomic data from the S-AKI and control groups was performed using the CIBERSORT algorithm (https://cibersort.stanford.edu/). We conducted immune infiltration analysis of the core targets using the bioinformatics platform (https://bioinformatics.com.cn/). The specific steps were as follows: First, the normalized gene expression matrix was uploaded to the CIBERSORT web tool; deconvolution analysis was then performed based on the LM22 (a signature gene expression matrix for 22 immune cell types); the number of permutations was set to 1000, and samples with $P < 0.05$ were retained as high-quality samples. Differences in the infiltration proportions of 22 immune cell types between

the S-AKI and control groups were compared using the Wilcoxon rank-sum test. The correlation between core gene expression and immune cell infiltration levels was assessed using Spearman's correlation coefficient.

2.10 Animal Housing and Cecal Ligation and Puncture Model Establishment

Specific pathogen-free (SPF) male C57BL/6 mice (6–8 weeks old, weighing 20–22 g) were purchased from Beijing Spaford Experimental Animal Company. All mice were housed in an SPF-grade animal facility under constant temperature (22–26°C), constant humidity (50 ± 10%), and a 12-hour light/dark cycle, with free access to food and water. Experiments commenced after 1 week of adaptive housing. Before surgery, mice were anesthetized with tribromoethanol (1.25% w/v in sterile saline) at a dose of 20ul/g body weight by intraperitoneal injection. The depth of anesthesia was confirmed by the absence of pedal reflex before surgery. An S-AKI mouse model was established using the cecal ligation and puncture (CLP) method. Mice were fasted for 12 hours prior to surgery with free access to water. After anesthesia induction with tribromoethanol, a longitudinal midline abdominal incision was made to expose the peritoneal cavity. The cecum was ligated with a 5-0 silk suture approximately 1 cm distal to the ileocecal valve, punctured twice with a 21G sterile needle, and a small amount of intestinal contents was extruded to ensure patency. The cecum was then returned to the abdominal cavity, and the incision was closed in layers. Immediately after surgery, pre-warmed sterile normal saline (50 mL/kg) was subcutaneously injected for fluid resuscitation, and mice were kept on a constant-temperature pad until recovery from anesthesia. Sham-operated mice (Sham group) underwent the same procedure except that the cecum was only exteriorized and then returned without ligation or puncture. At the end of the experiment, mice were euthanized by CO2 inhalation in a dedicated euthanasia chamber. CO2 was introduced gradually to displace chamber air and avoid rapid gas filling; exposure was continued until respiratory arrest and for at least 1 min thereafter, and death was confirmed by the absence of respiration and heartbeat before tissue collection. This procedure was performed in accordance with the AVMA Guidelines for the Euthanasia of Animals and the approved animal protocol and institutional guidelines. Sham-operated mice received the same anesthesia and euthanasia procedures.

All animal experiments were approved by the Animal Ethics Committee of Shanxi Medical University (Approval No. SYDL2026039). And all animal procedures were performed in accordance with the Guidelines for the Care and Use of Laboratory Animals (Ministry of Science and Technology of the People’s Republic of China, 2006)

and the NIH Guidelines for the Care and Use of Laboratory Animals (NIH Publication No. 85-23, revised 1996).

2.11 Renal Function Assessment

Serum creatinine and blood urea nitrogen measurement: At 24 hours post-CLP, approximately 0.5–1 mL of blood was collected from the orbital venous plexus. After standing at room temperature for 30 min, the blood was centrifuged at 3000 rpm for 15 min at 4°C, and the upper serum layer was separated. Serum creatinine (Cr) and blood urea nitrogen (BUN) levels were measured using a creatinine assay kit (sarcosine oxidase method) and a urea nitrogen assay kit (urease method), respectively. All procedures were performed strictly according to the manufacturers' instructions.

2.12 RNA Extraction and qPCR from Kidney Tissue

Approximately 30 mg of mouse kidney tissue was used for total RNA extraction via the TRIzol method. After reverse transcription to cDNA, real-time quantitative PCR (RT-qPCR) was performed using the SYBR Green method to detect the mRNA expression levels of NGAL and Hmgcs2, with β-actin as the internal reference. Primer sequences were synthesized by Shanghai Sangon Biotech. Relative expression levels were calculated using the 2^(-ΔΔCt) method.

2.13 Western Blotting for Renal Protein Expression

Approximately 30 mg of mouse kidney tissue was homogenized on ice in RIPA lysis buffer containing protease and phosphatase inhibitors. The homogenate was centrifuged at 12,000 rpm for 15 min at 4°C, and the supernatant was collected. Protein concentration was determined using the BCA method. Equal amounts of protein were separated by SDS-PAGE and transferred to PVDF membranes by wet electroblotting. After blocking with 5% non-fat milk at room temperature for 1 hour, membranes were incubated with the following primary antibodies: rabbit anti-Hmgcs2 (1:1000) and rabbit anti-mouse anti-β-actin (1:5000, internal reference) overnight at 4°C. After three washes with TBST, membranes were incubated with the corresponding HRP-conjugated secondary antibodies (1:5000) at room temperature for 1 hour. Following TBST washes, protein bands were visualized using ECL chemiluminescent substrate and imaged using a gel imaging system. Semi-quantitative analysis of band gray values was performed using ImageJ software, with relative target protein expression calculated as the ratio of target protein gray value to internal reference β-actin gray value. Note: We have now provided the original, unprocessed, and as full-length as possible blot images in the revised Supplementary Information (Supplementary Figure S1). We have also included an unannotated version of the original blots, while the annotated version is retained only for band localization. The main figure shows only the target band

regions because of space limitations, but the full original images are available in the Supplementary Information.

2.14 Renal Immunohistochemical Staining

Paraffin-embedded sections were dewaxed and rehydrated, followed by antigen retrieval through microwave heating in citrate buffer (pH 6.0) for 15 min. Endogenous peroxidase activity was blocked with 3% hydrogen peroxide for 10 min, and sections were blocked with 5% goat serum for 30 min. Sections were then incubated with rabbit anti-mouse Hmgcs2 primary antibody (dilution 1:200) overnight at 4°C. After PBS washes, sections were incubated with HRP-conjugated goat anti-rabbit secondary antibody (dilution 1:500) for 30 min at room temperature. Signals were developed using DAB chromogen, counterstained with hematoxylin, dehydrated, mounted, and observed under a microscope. PBS instead of primary antibody served as a negative control. Semi-quantitative analysis of positive staining area and optical density was performed using ImageJ software.

2.15 Statistical Analysis

All data are expressed as mean ± standard deviation (Mean ± SD). Statistical analyses were performed using GraphPad Prism 8.0 software. Comparisons between two groups were conducted using two-tailed unpaired Student's t-test.

3 Results

3.1 Identification of Differentially Expressed Genes in S-AKI

Based on the GSE60088 and GSE225192 datasets, with screening criteria of $|log2FC| > 1$ and $adj.P.Val < 0.05$, a total of 359 differentially expressed genes (DEGs) between the S-AKI and control groups were identified. The volcano plot displayed the overall distribution characteristics of these DEGs, with log2FC on the x-axis and -log10(adj.P.Val) on the y-axis; red and blue represented upregulated and downregulated DEGs, respectively, while gray represented genes without significant differences. The results showed that both upregulated and downregulated genes accounted for considerable proportions in the S-AKI group, suggesting extensive transcriptomic reprogramming in renal tissue during S-AKI (Fig1 A). The heatmap further illustrated the expression clustering patterns of the top 60 DEGs between the two groups, with rows representing genes and columns representing samples; red indicated high expression and blue indicated low expression. The clustering results revealed a clear separation between the S-AKI and control groups on the clustering dendrogram, further confirming the existence of substantial transcriptomic differences between the two groups (Fig1 B).

3.2 PPI Network Construction and Core Gene Screening

To clarify the interactions among proteins encoded by the DEGs, a PPI network was constructed based on the 359 DEGs, with “Degree” as the primary ranking metric to select targets with Degree > 1 for subsequent analyses. The results showed that this PPI network comprised 129 nodes (representing target proteins) and 232 edges (representing protein-protein interactions) (Fig1 C). Based on network topological features and node importance evaluation, Cxcl1, Ppara, Hmgcs2, Hmox1, Csf1, Fcgr3, Tufm, Lon2, Cd3, Timp1, Aif1, Cdk4, and Tufm were identified as core targets in the PPI network.

3.3 Functional Enrichment Analysis of DEGs

To explore the biological functions of the DEGs, GO functional annotation and KEGG pathway enrichment analyses were performed. GO analysis revealed that, in terms of BP, DEGs were significantly enriched in inflammatory response, immune regulation, cellular metabolic process, and mitochondrial organization. In terms of CC, DEGs were mainly enriched in mitochondria, cytoplasm, and nucleus. In terms of MF, significant enrichment was observed in oxidoreductase activity and transcription regulatory activity (Fig2 A). KEGG pathway enrichment analysis further revealed that these DEGs were primarily involved in fatty acid metabolism, oxidative phosphorylation, PPAR signaling pathway, as well as multiple inflammation-related pathways (such as TNF signaling pathway and NF-κB signaling pathway) (Fig2 B).

3.4 GSEA Analysis

To further reveal the overall transcriptomic trends in S-AKI at the pathway level, gene enrichment analysis was performed based on the ranking of all genes by expression. The results showed that multiple hallmark gene sets and KEGG pathways were significantly enriched in S-AKI. Among these, inflammation-related gene sets (e.g., IL6_JAK_STAT3_SIGNALING, TNFA_SIGNALING_VIA_NFKB) were significantly upregulated in the S-AKI group, whereas metabolism-related gene sets (e.g., FATTY_ACID_METABOLISM, OXIDATIVE_PHOSPHORYLATION) were significantly downregulated (Fig2 C-D). These findings further confirmed the critical roles of inflammatory response, metabolic reprogramming, and mitochondrial dysfunction in the pathogenesis of S-AKI.

3.5 LASSO Regression for Core Gene Screening

To further select the most discriminative feature genes from high-dimensional data, the LASSO regression algorithm was employed for feature selection. The optimal λ value was determined via ten-fold cross-validation, ultimately yielding 16 feature genes with

non-zero coefficients, including Angptl4, Zfp87, Gpr180, Dact1, Hdhd3, BC029722, Sptssa, Unc50, Timm10, Hmgcs2, Gsta4, C3, Mrps21, Mep1b, Mt2, and Timp1 (Fig3 A-B). These genes exhibited the most pronounced expression differences between S-AKI and control samples and carried the highest discriminative weights in the LASSO model.

3.6 Multi-dimensional Intersection Analysis Identifies Hmgcs2 as a Core Target

To precisely pinpoint key molecules in S-AKI, DEGs, LASSO-selected genes, lactate metabolism-related genes, and KEGG fatty acid metabolism pathway genes were subjected to Venn diagram intersection analysis. The four-set intersection ultimately identified Hmgcs2 (3-hydroxy-3-methylglutaryl-CoA synthase 2) as the sole core target gene (Fig4 A).

3.7 ROC Diagnostic Performance Evaluation of Hmgcs2

To evaluate the diagnostic value of Hmgcs2 for S-AKI, ROC curve analysis was performed. The results showed that Hmgcs2 could effectively distinguish the S-AKI group from the control group, with an AUC value greater than 0.7 ($P < 0.05$), indicating moderate to high diagnostic efficacy (Fig4 B-C). At the optimal cutoff value, both sensitivity and specificity reached reasonably ideal levels, suggesting that Hmgcs2 possesses the potential to serve as a biomarker for S-AKI.

3.8 Immune Infiltration Analysis

We further utilized the CIBERSORT algorithm to assess differences in immune cell infiltration between the S-AKI and control groups. The results showed that the infiltration proportions of multiple immune cell types were significantly altered in the S-AKI group (Fig5 A-B). Compared with the control group, the proportions of M0 macrophages and neutrophils were significantly increased in the S-AKI group, whereas the proportions of certain T cell subsets (e.g., $CD8^+$ T cells) were decreased. These changes were consistent with the pathological features of aggravated inflammatory responses and remodeling of the immune microenvironment in S-AKI. Further correlation analysis revealed that Hmgcs2 expression levels were significantly associated with the infiltration proportions of specific immune cells: samples with high Hmgcs2 expression tended to show a balanced M1/M2 macrophage ratio, whereas samples with low Hmgcs2 expression exhibited more pronounced pro-inflammatory immune cell infiltration (Fig5 C). This result suggested that Hmgcs2 may participate in the pathological process of S-AKI by modulating the renal immune microenvironment.

3.9 *In Vivo* Experimental Validation of Hmgcs2 Upregulation in Renal Tissue of CLP-Induced S-AKI Mice

To verify the reliability of the bioinformatics screening results, we established a CLP-induced S-AKI mouse model. At 24 hours post-CLP, serum BUN and Cr levels in the model group were significantly higher than those in the sham-operated group, indicating successful S-AKI model establishment (Fig6 A-B). Meanwhile, RT-qPCR analysis showed that the mRNA level of the renal injury marker NGAL in renal tissue was significantly upregulated in the model group (Fig6 C). On this basis, we further examined the expression changes of Hmgcs2 in S-AKI renal tissue. RT-qPCR results demonstrated that, compared with the sham group, Hmgcs2 mRNA levels in renal tissue of CLP model mice were significantly elevated (Fig6 D). Western blotting results further confirmed that Hmgcs2 protein expression in renal tissue of the model group was markedly upregulated, with ImageJ quantification showing an approximately 2.5-fold increase in relative expression compared with the sham group (Fig6 E-F). Immunohistochemical staining revealed that Hmgcs2 was barely detectable in renal tissue of sham-operated mice, whereas strongly positive Hmgcs2 staining, mainly localized in the cytoplasm, was observed in renal proximal tubules of CLP model mice (Fig6 G). Collectively, these results indicated that Hmgcs2 was significantly upregulated at both mRNA and protein levels in the CLP-induced S-AKI mouse model, not only corroborating the predictions from bioinformatics analyses but also suggesting that Hmgcs2 may be involved in the pathophysiological processes of S-AKI.

4 Discussion

In this study, by integrating two mouse kidney transcriptomic datasets from the GEO database, combined with differential expression analysis, functional enrichment analysis, PPI network construction, and LASSO machine learning algorithm, we systematically screened for key genes in S-AKI. Based on the intersection analysis of DEGs, LASSO-derived feature genes, fatty acid metabolism pathway genes, and lactate metabolism-related genes, Hmgcs2 was identified as the core target. Its diagnostic value and immunomodulatory potential were further evaluated through ROC curve and immune infiltration analyses. It should be noted that the “lactylation-related gene set” referred to in this study denotes the gene network regulated by lactate metabolites, rather than the lactylation modification of the Hmgcs2 protein per se. The rationale for introducing the lactate metabolism-related gene set instead of directly using the lactylation modification gene set is that, at present, there is no well-established database for lactylation modification genes, whereas the lactate metabolism-related gene set can indirectly reflect the changes in lactate levels and the activity of the lactate metabolic

pathway, thereby providing a metabolic entry point for subsequent exploration of lactylation modification. Finally, the upregulation of Hmgcs2 expression in renal tissue was verified in a CLP-induced S-AKI mouse model. This study is the first to reveal the potential protective role of Hmgcs2 in S-AKI from the perspective of the interplay between fatty acid metabolism and lactylation modification, providing a new perspective for mechanistic research and clinical translation of S-AKI.

The pathogenesis of S-AKI involves the interplay of multiple pathological processes, including inflammatory dysregulation, metabolic reprogramming, and mitochondrial dysfunction[5]. To uncover the molecular landscape of S-AKI, this study first identified a total of 359 significantly altered genes in S-AKI through DEG analysis. GO/KEGG enrichment analysis revealed that these genes were significantly enriched in terms such as inflammatory response, fatty acid metabolism, oxidative phosphorylation, and the PPAR signaling pathway, while GSEA further confirmed that inflammation-related gene sets were significantly upregulated in S-AKI, whereas FAO and oxidative phosphorylation gene sets were significantly downregulated—which is fully consistent with the core pathological features of "FAO suppression and inflammation activation" in S-AKI[25]. Notably, the emergence of the PPAR signaling pathway is particularly critical: PPARα is the major transcriptional regulator of FAO, and its deficiency leads to reduced FAO and worsening of renal function, whereas the PPARα agonist fenofibrate has been shown to attenuate S-AKI by enhancing renal FAO[3,13]. PPI network analysis further identified core nodes such as Ppara, Hmgcs2, Cxcl1, and Hmox1, among which the association between Ppara and Hmgcs2 has a clear regulatory biological basis—Hmgcs2 is a direct downstream target gene of PPARα, and its promoter region contains functional PPAR response elements[26]. Collectively, the above analyses, at the levels of transcriptome, functional pathways, and protein-protein interactions, consistently point to the potential core status of the Ppara–Hmgcs2 regulatory axis in S-AKI.

On this basis, we introduced the LASSO machine learning algorithm for feature selection to extract the most discriminative key genes from high-dimensional data[27]. Through ten-fold cross-validation, LASSO regression compressed the candidate genes from 359 DEGs to 16 core feature genes. To more precisely pinpoint molecules simultaneously involved in both fatty acid metabolism and lactylation modification—two key processes—we performed a four-way Venn diagram intersection analysis among DEGs, LASSO-selected feature genes, KEGG fatty acid metabolism pathway genes, and lactate metabolism-related genes, and the sole overlapping gene was

Hmgcs2. Hmgcs2 (3-hydroxy-3-methylglutaryl-CoA synthase 2) is the rate-limiting enzyme of ketogenesis; its substrates, acetyl-CoA and acetoacetyl-CoA, are both derived from fatty acid β-oxidation, so its activity is closely coupled with FAO[28,29]. In recent years, the tissue-specific functions of Hmgcs2 in the kidney have been increasingly recognized: unlike hepatic Hmgcs2, which contributes to systemic circulating ketone bodies, renal Hmgcs2 mainly acts locally[30]. In ischemic kidney injury, upregulation of proximal tubular Hmgcs2 increases local ketone body content in the kidney and exerts a protective effect, whereas Hmgcs2-deficient mice exhibit more severe kidney injury and impaired FAO capacity[31]. This functional positioning of “local protection rather than systemic energy supply” makes Hmgcs2 a candidate molecule worthy of in-depth investigation in S-AKI.

ROC curve analysis showed that Hmgcs2 exhibited good diagnostic performance (AUC > 0.7), suggesting its potential as a biomarker for S-AKI. Immune infiltration analysis revealed that the infiltration of pro-inflammatory immune cells such as macrophages M0 and neutrophils was significantly increased in the S-AKI group, and Hmgcs2 expression levels were significantly correlated with macrophage polarization status—samples with high Hmgcs2 expression tended toward a balanced M1/M2 ratio, whereas samples with low expression displayed more pronounced pro-inflammatory infiltration. This finding echoes the known functions of Hmgcs2 in immune regulation: in septic myocardial injury, Hmgcs2 promotes macrophage M2 polarization to exert a reparative role[32]; in diabetic kidney disease, Hmgcs2 mediates tubule-macrophage inflammatory crosstalk[33]. To validate the bioinformatics predictions, we established a CLP-induced S-AKI mouse model and examined Hmgcs2 expression in renal tissue. The results showed that both mRNA and protein levels of Hmgcs2 were significantly upregulated in S-AKI renal tissues, and immunohistochemical staining confirmed that it was mainly localized in the cytoplasm of proximal tubules. This expression pattern is consistent with previous reports: Hmgcs2 is nearly undetectable in normal kidneys but is markedly induced in proximal tubules under septic and fasting conditions in a PPARα-dependent manner[34]. Collectively, the immune analysis results and in vivo experiments robustly validate the close association between Hmgcs2 and S-AKI from multiple dimensions.

The most central scientific question of this study is: why was Hmgcs2 screened out through the intersection of the two dimensions of "fatty acid metabolism" and "lactate metabolism-related gene sets"? The answer lies in the unique dual functional positioning of Hmgcs2. On the one hand, as a key enzyme downstream of FAO,

Hmgcs2 is directly involved in renal energy metabolism, and its catalytic product β-hydroxybutyrate (β-OHB) serves as a direct donor for histone β-hydroxybutyrylation (Kbhb), thereby participating in epigenetic regulation[35,36]. On the other hand, lactate, as a signaling molecule, can influence the substrate availability and transcriptional regulation of Hmgcs2 by modulating the intracellular acetyl-CoA/NADH ratio. Notably, β-hydroxybutyrate (β-OHB) produced by the catalytic action of Hmgcs2 can mediate histone β-hydroxybutyrylation (Kbhb), which is a modification type belonging to the same metabolite–epigenetic conversion family as lactylation. The two modifications share modification sites on lysine residues and may have a competitive antagonistic relationship[37,38]. The essence of lactylation is the metabolite–epigenetic conversion from lactate to lysine lactylation, whereas the ketogenesis pathway in which Hmgcs2 is involved mediates a similar conversion from fatty acids to β-OHB and then to Kbhb[36,39,40]. Both modifications occur on lysine residues and are regulated by intracellular metabolite concentrations, suggesting that there may be a competitive relationship between them[41]. Based on these observations, we propose the following hypothesis: in S-AKI, FAO suppression leads to enhanced glycolysis and lactate accumulation, which upregulates lactylation and mediates pathological effects; meanwhile, upregulation of Hmgcs2 enhances Kbhb modification by increasing β-OHB production, potentially antagonizing the pathological role of lactylation at the same modification sites, thereby establishing a buffering barrier between metabolic derangement and epigenetic dysregulation. This hypothesis provides a novel perspective for understanding the protective mechanism of Hmgcs2, but still requires validation through site-specific modification antibodies and competitive experiments.

Several limitations exist in this study. First, this study is mainly based on bioinformatics analysis and machine learning algorithms; all core findings are computational predictions, and the specific protective functions and molecular mechanisms of Hmgcs2 in S-AKI still need to be further validated through gene knockout or overexpression animal experiments and cellular functional assays. Second, whether Hmgcs2 indeed exerts its role in S-AKI through the two major pathways of fatty acid oxidation (FAO) and lactylation modification still requires direct evidence from metabolic flux analysis, lactylation detection, and pathway intervention experiments, and currently this mechanistic inference lacks experimental support. Finally, the mouse model data used in this study have species differences compared with clinical S-AKI patients, and the sample size is limited; caution should be exercised when extrapolating the findings to human S-AKI. Future research should focus on: using kidney-specific

Hmgcs2 knockout mice to clarify its functional direction in S-AKI; systematically dissecting the downstream metabolic networks and epigenetic modification changes regulated by Hmgcs2 through metabolomics and modificomics; validating Hmgcs2 expression changes, diagnostic efficacy, and its association with prognosis in larger clinical S-AKI patient cohorts; and exploring the therapeutic potential of intervention strategies targeting Hmgcs2 and its metabolic pathways in S-AKI.

5 Conclusion

Through integrative multi-dataset transcriptomic analysis, functional enrichment analysis, PPI network analysis, and the LASSO machine learning algorithm, this study systematically screened for key genes of S-AKI. Combined with multi-dimensional intersection analysis using the KEGG fatty acid metabolism pathway gene set and lactate metabolism-related gene set, Hmgcs2 was ultimately identified as the sole core target. As the rate-limiting enzyme of ketogenesis, Hmgcs2 lies at the intersection of two major biological processes: fatty acid metabolism and lactylation modification. On the one hand, Hmgcs2 participates in renal energy metabolism through FAO; on the other hand, it may indirectly participate in epigenetic regulation related to lactylation modification by influencing the metabolic microenvironment. This study is the first to reveal the potential core role of Hmgcs2 in S-AKI from the perspective of the interplay between fatty acid metabolism and lactylation modification, providing new ideas for mechanistic research and clinical translation of S-AKI. Hmgcs2 holds promise as a biomarker for the diagnosis of S-AKI and a potential target for targeted therapy, but its specific functional mechanisms require further experimental validation.

Funding

This study was supported by the Shanxi Provincial Natural Science Research General Program (202403021211123, 202403021211124), the College Students' Innovation and Entrepreneurship Training Program of Shanxi Province (20250425, 20260738, 20260846).

Author contributions

Jinzhi SONG: investigation, validation, visualization, methodology; Yawen WU: writing-review & editing, writing-original draft, validation, methodology, investigation, funding acquisition; Gehui XIAO: validation, software; Xueqin LI & Hongmei ZHANG: formal analysis; Na XIA: investigation, funding acquisition; Jianying BAI: writing-review & editing, supervision, conceptualization, funding acquisition; Xuan SHANG: supervision, methodology, software, writing-review & editing, funding acquisition.

Declarations

Ethics statement

All animal experiments were approved by the Animal Ethics Committee of Shanxi Medical University (Approval No. SYDL2026039). All animal procedures were performed in accordance with the Guidelines for the Care and Use of Laboratory Animals (Ministry of Science and Technology of the People's Republic of China, 2006) and the NIH Guidelines for the Care and Use of Laboratory Animals (NIH Publication No. 85-23, revised 1996).

Consent to participate

Not applicable. This study did not involve human participants.

Consent to publish

Not applicable. This manuscript does not contain data from any individual person.

Conflict of interest statement

All authors declare that they have no conflicts of interest.

Data availability statement

The datasets used and/or analyzed in this study are available from the corresponding author upon reasonable request. The transcriptomic datasets analyzed in this study are publicly available in the Gene Expression Omnibus (GEO) repository under accession numbers GSE60088 and GSE225192. The original uncropped and unprocessed gel/blot images and the data generated in this study are included in the Supplementary Information and are available from the corresponding author on reasonable request.

Acknowledgements

This work was financially supported by the Shanxi Provincial Natural Science Research General Program (Grant Nos. 202403021211123 and 202403021211124) and the College Students' Innovation and Entrepreneurship Training Program of Shanxi Province (Grant Nos. 20250425, 20260738, and 20260846).

Clinical trial number: not applicable.

References

1. Shi B, Ye J, Chen W, Liao B, Gu W, Yin H, et al. Prognosis of critically ill patients with early and late sepsis-associated acute kidney injury: an observational study based on the MIMIC-IV. Ren Fail. 2025 Dec;47(1):2441393. doi:10.1080/0886022X.2024.2441393 PubMed PMID: 39980278; PubMed Central PMCID: PMC11849006.
2. Takeuchi T, Flannery AH, Liu LJ, Ghazi L, Cama-Olivares A, Fushimi K, et al. Epidemiology of sepsis-associated acute kidney injury in the ICU with contemporary consensus definitions. Crit Care. 2025 Mar 20;29(1):128. doi:10.1186/s13054-025-05351-5 PubMed PMID: 40114218; PubMed Central PMCID: PMC11924826.
3. Zeng S, Wang J, Guan C, Yao Z, Zhang Y, Li Y, et al. Fenofibrate alleviates sepsis-associated acute kidney injury by enhancing renal fatty acid oxidation. BMC Pharmacol Toxicol. 2025 Oct 7;26(1):160. doi:10.1186/s40360-025-00997-x PubMed PMID: 41057888; PubMed Central PMCID: PMC12505558.
4. Liu AB, Tan B, Yang P, Tian N, Li JK, Wang SC, et al. The role of inflammatory response and metabolic reprogramming in sepsis-associated acute kidney injury: mechanistic insights and therapeutic potential. Front Immunol. 2024;15:1487576. doi:10.3389/fimmu.2024.1487576 PubMed PMID: 39544947; PubMed Central PMCID: PMC11560457.
5. Liu C, Wei W, Huang Y, Fu P, Zhang L, Zhao Y. Metabolic reprogramming in septic acute kidney injury: pathogenesis and therapeutic implications. Metabolism. 2024 Sep;158:155974. doi:10.1016/j.metabol.2024.155974 PubMed PMID: 38996912.
6. Wang T, Huang Y, Zhang X, Zhang Y, Zhang X. Advances in metabolic reprogramming of renal tubular epithelial cells in sepsis-associated acute kidney injury. Front Physiol. 2024;15:1329644. doi:10.3389/fphys.2024.1329644 PubMed PMID: 38312312; PubMed Central PMCID: PMC10834781.
7. Wang C, Liu Q, Wang H, Zhang Q, Yang B, Liu H, et al. Mitochondrial dysfunction in sepsis-

associated acute kidney injury: mechanisms and therapeutic potential. Front Immunol. 2026;17:1829288. doi:10.3389/fimmu.2026.1829288 PubMed PMID: 42238588; PubMed Central PMCID: PMC13226585.

8. Simon N, Hertig A. Alteration of Fatty Acid Oxidation in Tubular Epithelial Cells: From Acute Kidney Injury to Renal Fibrogenesis. Front Med (Lausanne). 2015;2:52. doi:10.3389/fmed.2015.00052 PubMed PMID: 26301223; PubMed Central PMCID: PMC4525064.
9. ZHENG X, ZHOU F, LUO Q. Metabolic reprogramming of proximal renal tubular epithelial cells in acute kindey injury. Chinese Journal of Nephrology, Dialysis & Transplantation. 2024 Feb 28;33(1):59. doi:10.3969/j.issn.1006-298X.2024.01.012
10. Console L, Scalise M, Giangregorio N, Tonazzi A, Barile M, Indiveri C. The Link Between the Mitochondrial Fatty Acid Oxidation Derangement and Kidney Injury. Front Physiol. 2020;11:794. doi:10.3389/fphys.2020.00794 PubMed PMID: 32733282; PubMed Central PMCID: PMC7363843.
11. Schaub JA, Venkatachalam MA, Weinberg JM. Proximal Tubular Oxidative Metabolism in Acute Kidney Injury and the Transition to CKD. Kidney360. 2021 Feb 25;2(2):355–64. doi:10.34067/KID.0004772020 PubMed PMID: 35373028; PubMed Central PMCID: PMC8740982.
12. Standage SW, Xu S, Brown L, Ma Q, Koterba A, Lahni P, et al. NMR-based serum and urine metabolomic profile reveals suppression of mitochondrial pathways in experimental sepsis-associated acute kidney injury. Am J Physiol Renal Physiol. 2021 May 1;320(5):F984–1000. doi:10.1152/ajprenal.00582.2020 PubMed PMID: 33843271; PubMed Central PMCID: PMC8424559.
13. Iwaki T, Bennion BG, Stenson EK, Lynn JC, Otinga C, Djukovic D, et al. PPARα contributes to protection against metabolic and inflammatory derangements associated with acute kidney injury in experimental sepsis. Physiol Rep. 2019 May;7(10):e14078. doi:10.14814/phy2.14078 PubMed PMID: 31102342; PubMed Central PMCID: PMC6525329.
14. Song L, Jiang W, Liu K, Wang J, Gong W, Yu J, et al. Post-translational modifications in sepsis-induced acute kidney injury: mechanisms and perspectives. Front Pharmacol. 2025;16:1625139. doi:10.3389/fphar.2025.1625139 PubMed PMID: 40989844; PubMed Central PMCID: PMC12450668.
15. Zhang S, Luo M, Lu Z, Shi Q. Lactate and lactylation in sepsis-associated acute kidney injury: clinical evidence from the MIMIC-IV database and mechanistic insights. Front Med (Lausanne). 2025;12:1708145. doi:10.3389/fmed.2025.1708145 PubMed PMID: 41322213; PubMed Central PMCID: PMC12660216.
16. Zheng J, Zheng B, Liang Q. Lactylation in Sepsis-Associated Acute Kidney Injury: Regulatory Mechanisms and Therapeutic Prospects. Front Mol Biosci. 2026 Jul 16;13. doi:10.3389/fmolb.2026.1899336
17. Payen D, Rimmelé T, Gómez H. Hyperlactatemia in sepsis and shock: a renal metabolic perspective. Crit Care. 2026 Jun 3. doi:10.1186/s13054-026-06095-6 PubMed PMID: 42237139.
18. Huang Y, Zhao E, Zhao G, Zhuo W, Zhao Y, Wang H, et al. H3K18 lactylation-mediated SPHK1-SIRT1 feedback loop accelerates pyroptosis of tubular epithelial cells in sepsis-associated acute kidney injury. Theranostics. 2026;16(9):4768–86. doi:10.7150/thno.122991 PubMed PMID: 41799201; PubMed Central PMCID: PMC12964219.

19. Wei X, Xiao G, Chen X, Zhang J, Xu Q. Expanding the plant epigenetic code: histone short-chain acylation. Trends Plant Sci. 2026 Feb;31(2):221–37. doi:10.1016/j.tplants.2025.10.020 PubMed PMID: 41298197.
20. Trefely S, Lovell CD, Snyder NW, Wellen KE. Compartmentalised acyl-CoA metabolism and roles in chromatin regulation. Mol Metab. 2020 Aug;38:100941. doi:10.1016/j.molmet.2020.01.005 PubMed PMID: 32199817; PubMed Central PMCID: PMC7300382.
21. Chen Y, Wang Y, Ning X, Xu J. LDHA-driven ACAA2 lactylation at K270 reprograms fatty acid metabolism to promote clear cell renal cell carcinoma progression. Sci Rep. 2026 Apr 20;16(1):18406. doi:10.1038/s41598-026-46158-w PubMed PMID: 42009890; PubMed Central PMCID: PMC13266038.
22. Zehra null, Bakhtiyar A, Islam A, Ishrat R, Hassan MI. AI-driven approaches in therapeutic interventions: Transforming RNA-seq analysis into biomarker discovery and drug development. Drug Discov Today. 2025 Jul;30(7):104391. doi:10.1016/j.drudis.2025.104391 PubMed PMID: 40449581.
23. He Z, Ma H, Zhang Y, Chen L, Pang Y, Ding X, et al. Identification of Npas4 as a biomarker for CICI by transcriptomics combined with bioinformatics and machine learning approaches. Exp Neurol. 2025 Sep;391:115290. doi:10.1016/j.expneurol.2025.115290 PubMed PMID: 40340014.
24. Zhou P, Li Z, Liu F, Kwon E, Hsieh TC, Ye S, et al. BAMBI integrates biostatistical and artificial intelligence methods to improve RNA biomarker discovery. Brief Bioinform. 2025 Mar 4;26(2):bbaf073. doi:10.1093/bib/bbaf073 PubMed PMID: 40121554; PubMed Central PMCID: PMC11929966.
25. Zeng S, Yao Z, Guan C, Zhang Y, Cui S, Quan Z, et al. Ketogenic diet mitigates sepsis‐associated acute kidney injury in mice via reactivation of fatty acid oxidation: a multi‐omics and mechanistic study. Food Science and Human Wellness. 2026 Jan 28. doi:10.26599/FSHW.2026.9250923
26. Kostiuk MA, Keller BO, Berthiaume LG. Palmitoylation of ketogenic enzyme HMGCS2 enhances its interaction with PPARalpha and transcription at the Hmgcs2 PPRE. FASEB J. 2010 Jun;24(6):1914–24. doi:10.1096/fj.09-149765 PubMed PMID: 20124434; PubMed Central PMCID: PMC2874477.
27. Baek B, Jo J, Kang M, Kim Y. Stochastic LASSO for extremely high-dimensional genomic data. Sci Rep. 2026 Jan 14;16(1):5250. doi:10.1038/s41598-026-35273-3 PubMed PMID: 41535372; PubMed Central PMCID: PMC12881642.
28. Conboy E, Vairo F, Schultz M, Agre K, Ridsdale R, Deyle D, et al. Mitochondrial 3-Hydroxy-3-Methylglutaryl-CoA Synthase Deficiency: Unique Presenting Laboratory Values and a Review of Biochemical and Clinical Features. JIMD Rep. 2018;40:63–9. doi:10.1007/8904_2017_59 PubMed PMID: 29030856; PubMed Central PMCID: PMC6122033.
29. Han X, Wang K, Ma W, Zhu S, Guan J, Tian X, et al. A ketogenesis-ferroptosis axis maintains leukemic stem cell survival and leukemia progression. Cell Stem Cell. 2026 Jun 4;33(6):1016-1030.e6. doi:10.1016/j.stem.2026.04.013 PubMed PMID: 42119562.
30. Junya H, Sho S, Mako Y, Kosuke Y, Shogo K, Yuki T, et al. Physiological Role of Renal Ketogenesis: SA-PO0491. Journal of the American Society of Nephrology. 2025 Oct;36(10S):SA-PO049. doi:10.1681/ASN.2025jwcbpmpb
31. Feola K, Venable AH, Rasouli M, Haley EG, Jadhav C, Monroy R, et al. Renal Ketogenesis

Protects Against Ischemic Kidney Injury. J Am Soc Nephrol. 2026 Aug 1;37(8):1628–42. doi:10.1681/ASN.0000001014 PubMed PMID: 41568909; PubMed Central PMCID: PMC12952000.

32. Zou XZ, Hao JF, Hou MX. Hmgcs2 regulates M2 polarization of macrophages to repair myocardial injury induced by sepsis. Aging (Albany NY). 2023 Aug 9;15(15):7794–810. doi:10.18632/aging.204944 PubMed PMID: 37561521; PubMed Central PMCID: PMC10457052.

33. Lin Z, Lv D, Zha H, Liu H, Peng R, Yang J, et al. HMGCS2 desuccinylation modulates acetoacetate to drive tubule-macrophage inflammatory crosstalk in diabetic kidney disease. Metabolism. 2026 Apr;177:156510. doi:10.1016/j.metabol.2026.156510 PubMed PMID: 41580118.

34. Nakano D, Kittikulsuth W, Nishiyama A. The Role of Renal Hmgcs2 in Fasting and Bacterial Inflammation: PO0373. Journal of the American Society of Nephrology. 2021 Oct;32(10S):161–161. doi:10.1681/ASN.20213210S1161a

35. Funk SD, Kern JT, Viquez OM, Sulvaran-Guel E, Koenitzer JR, Feola KC, et al. Tubule-Specific Compensatory Responses to Cpt1a Deletion in Aged Mice. Kidney360. 2025 May 1;6(5):707–19. doi:10.34067/KID.0000000746 PubMed PMID: 40138521; PubMed Central PMCID: PMC12136631.

36. Chen Y, Cao A, Fan Y, Wang N. HMGCS2 Drives Mitochondrial Reprogramming and Histone β-Hydroxybutyrylation in Diabetic Nephropathy FR-PO0319. Journal of the American Society of Nephrology. 2025 Oct;36(10S):FR-PO0319. doi:10.1681/ASN.20257gws3v66

37. Qi W, Su J, He X, Yang F, Li Q, Li B. Crosstalk between lactylation and other post-translational modifications in health and diseases. Mol Biomed. 2026 Jul 16;7(1):112. doi:10.1186/s43556-026-00500-w PubMed PMID: 42461359; PubMed Central PMCID: PMC13376120.

38. Fu Z, Shi R, Jiang L, Zhang W, Liu Y, Chen W, et al. Lactylation in concert with other post-translational modifications: Regulatory networks and disease implications. Cell Investigation. 2026 Jun;2(2):100078. doi:10.1016/j.clnves.2026.100078

39. Terranova CJ, Stemler KM, Barrodia P, Jeter-Jones SL, Ge Z, de la Cruz Bonilla M, et al. Reprogramming of H3K9bhb at regulatory elements is a key feature of fasting in the small intestine. Cell Rep. 2021 Nov 23;37(8):110044. doi:10.1016/j.celrep.2021.110044 PubMed PMID: 34818540; PubMed Central PMCID: PMC8668154.

40. Zhang Y, Chen L, Qin Y, Wang Y, Liu X, Zhang M, et al. Lactylation in cancer: a new frontier in metabolic-epigenetic regulation and clinical practice. Cell Commun Signal. 2026 Jul 24. doi:10.1186/s12964-026-03085-7

41. Chen C, Chen X, Lyu X, Yao L, Ge S, Yu M, et al. Lysine β-hydroxybutyrylation: A metabolic-epigenetic interface in health and disease. Phytomedicine. 2026 Aug;158:158410. doi:10.1016/j.phymed.2026.158410 PubMed PMID: 42284641.

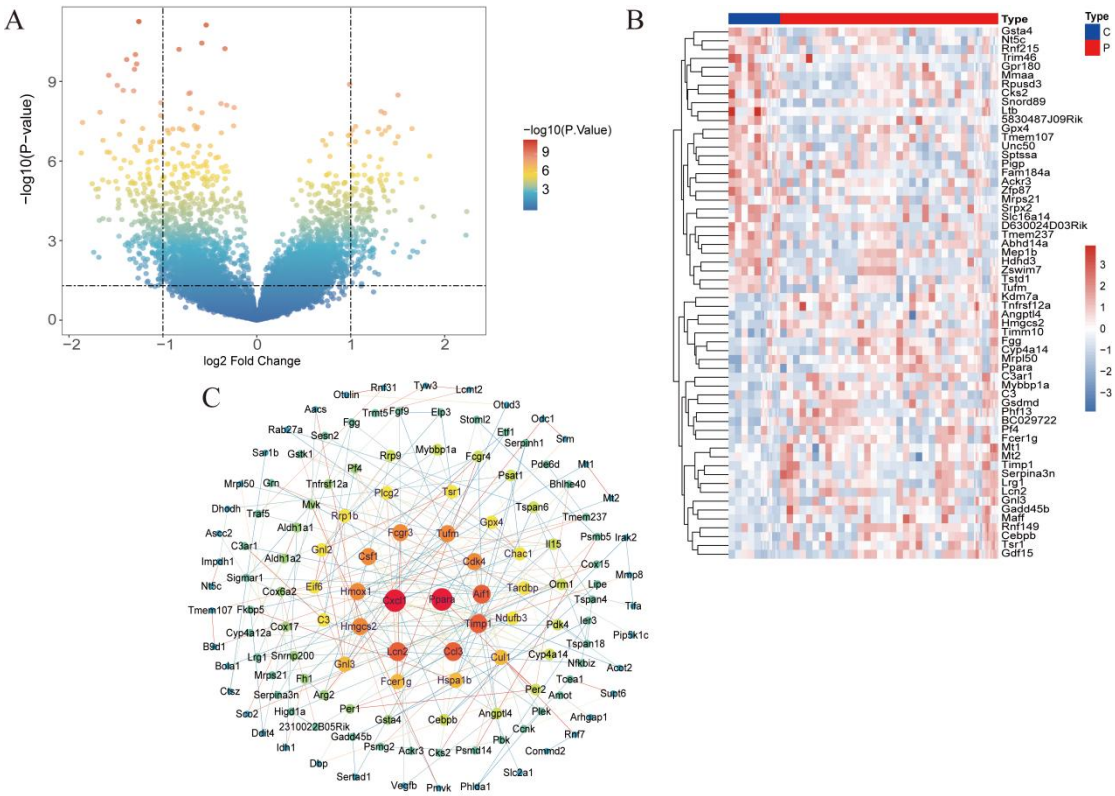


Figure 1 Identification of DEGs in S-AKI and PPI network analysis

(A) Volcano plot showing the distribution of DEGs between the S-AKI group and the control group. The horizontal axis represents $\log_2$ (fold change), and the vertical axis represents $-\log_{10}$ (adjusted *P*-value). Red dots denote significantly upregulated genes, blue dots denote significantly downregulated genes, and grey dots denote genes with no significant difference (filtering criteria: $|\log_2 FC| > 1$ and adj.*P*.Val < 0.05).

(B) Heatmap displaying the clustering pattern of the top 60 DEGs between the S-AKI group and the control group. Rows represent genes, columns represent samples; red indicates high expression, and blue indicates low expression.

(C) PPI network diagram of DEGs constructed based on the STRING database. Nodes represent proteins/genes, edges represent protein–protein interactions, node size reflects the degree of connectivity, and color intensity reflects the score calculated by the MCC algorithm.

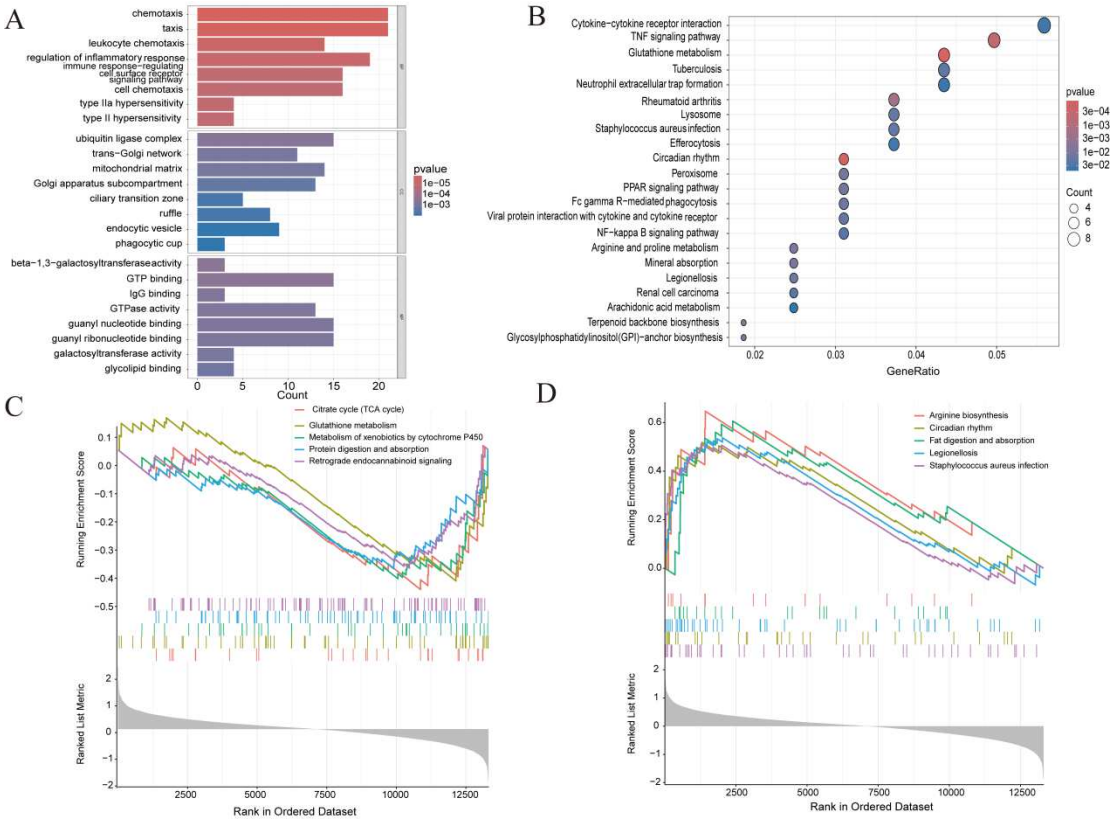


Figure 2 Functional enrichment analysis and GSEA based on DEGs

(A) Bar plot of GO functional enrichment analysis, showing the top 8 significantly enriched terms in the three ontologies: biological process (BP), cellular component (CC), and molecular function (MF).

(B) Bubble plot of KEGG pathway enrichment analysis, showing significantly enriched signaling pathways among DEGs. Bubble size represents the number of enriched genes, and color represents the significance of enrichment (*P*-value).

(C–D) GSEA enrichment analysis displaying the enrichment of hallmark gene sets in the S-AKI group. Red indicates significantly upregulated pathways in the S-AKI group, and blue indicates significantly downregulated pathways (FDR < 0.25, $P < 0.05$).

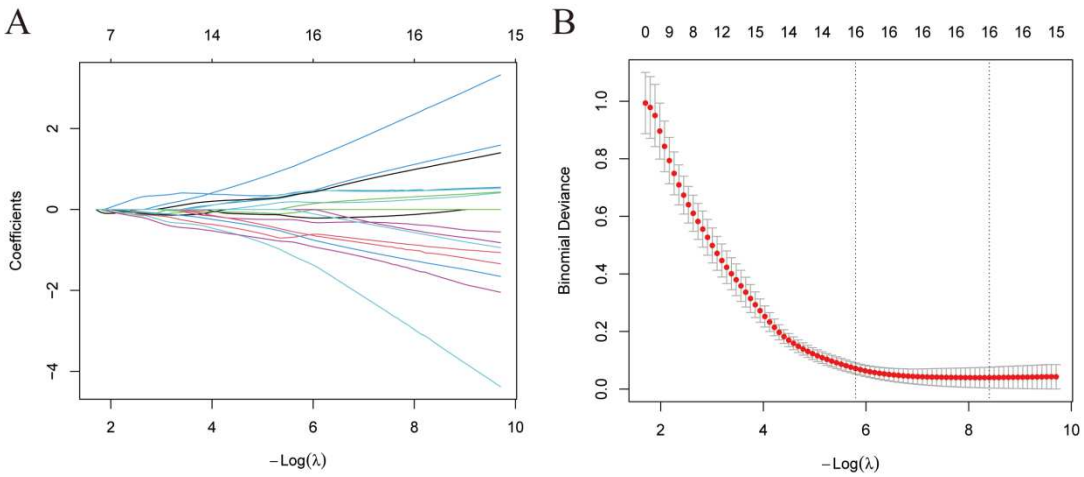


Figure 3 LASSO regression for screening core signature genes

(A) Variation curve of mean squared error (MSE) corresponding to different λ values in the LASSO regression model. The vertical axis represents cross-validation deviance, and the horizontal axis represents log(λ). The left dashed line corresponds to λ.min (the λ value at minimum deviance), and the right dashed line corresponds to λ.1se (the largest λ within one standard error of the minimum deviance).

(B) Coefficient trajectory plot of each gene in the LASSO regression model. Each curve represents the change in regression coefficient of a gene under different λ values; genes with non-zero coefficients at the final selection are retained.

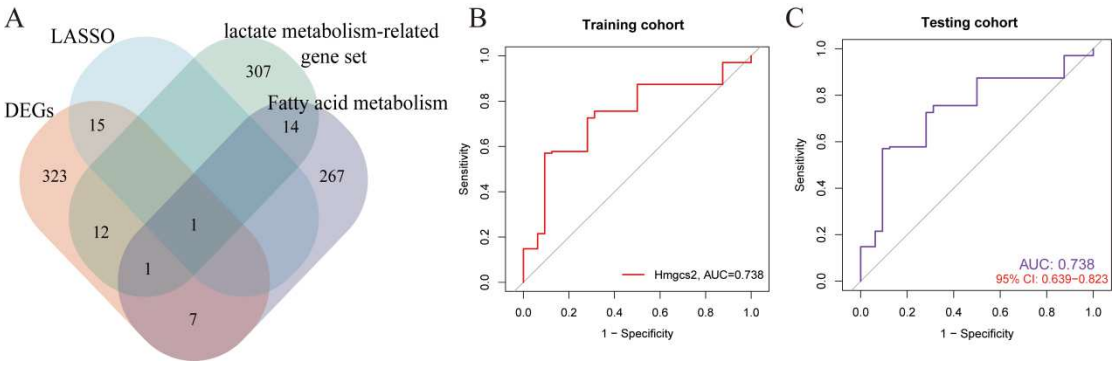


Figure 4 Venn diagram intersection analysis for identification of core target and evaluation of diagnostic performance.

(A) Venn diagram intersection analysis of differentially expressed genes (DEGs), LASSO-selected genes, a lactate metabolism-related gene set, and KEGG fatty acid metabolism pathway genes. The overlapping region (center) of the four ellipses represents Hmgcs2, the only core target simultaneously belonging to all four gene groups.

(B) Univariate ROC curve of Hmgcs2 for evaluating its diagnostic value for S-AKI. The AUC is 0.738, with sensitivity and specificity annotated in the figure, indicating moderate diagnostic performance.

(C) ROC curve of a predictive model based on multivariate analysis (including Hmgcs2 and other clinical indicators) for evaluating the combined diagnostic capability.

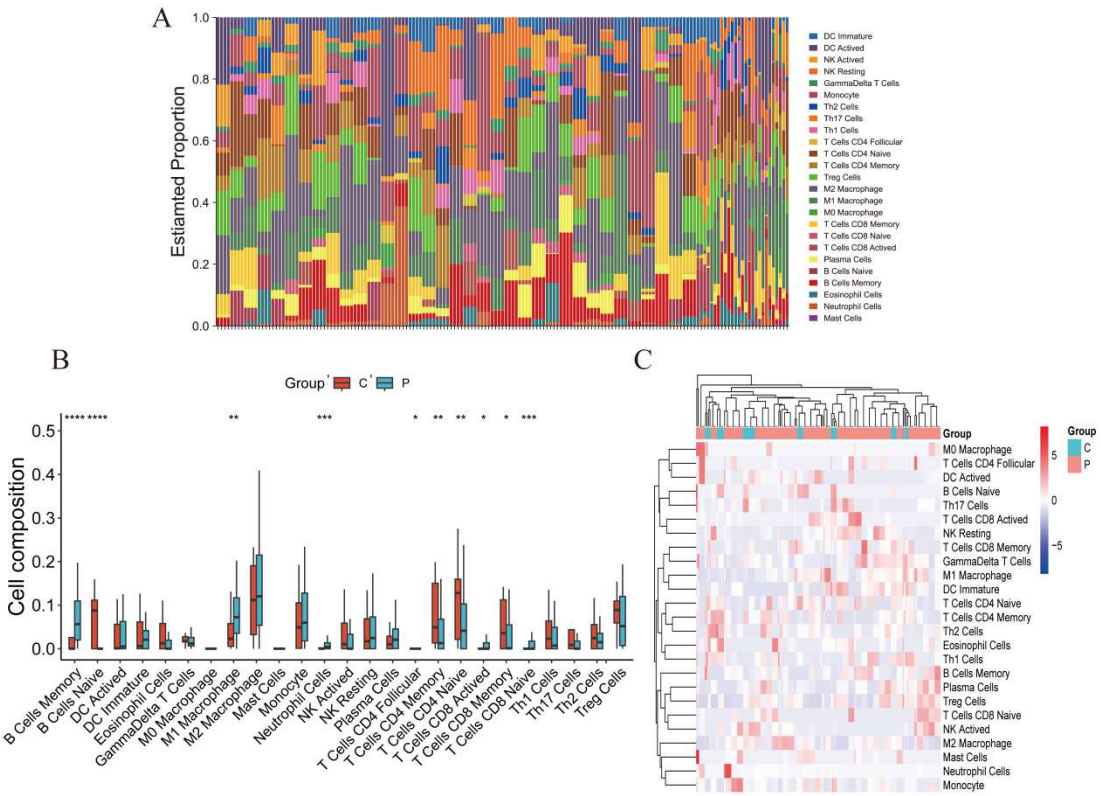


Figure 5 Immune infiltration analysis

(A) Stacked bar plot of the infiltration proportions of 22 immune cell types estimated by the CIBERSORT algorithm between the S-AKI group and the control group. Each color represents one immune cell type.

(B) Boxplot comparing immune cell types with significant differences between the S-AKI group and the control group.

(C) Spearman correlation heatmap between Hmgcs2 expression level and infiltration proportions of key immune cells (e.g., macrophages M0, neutrophils) in the S-AKI group, showing correlation coefficients and significance levels; red indicates positive correlation, and blue indicates negative correlation.

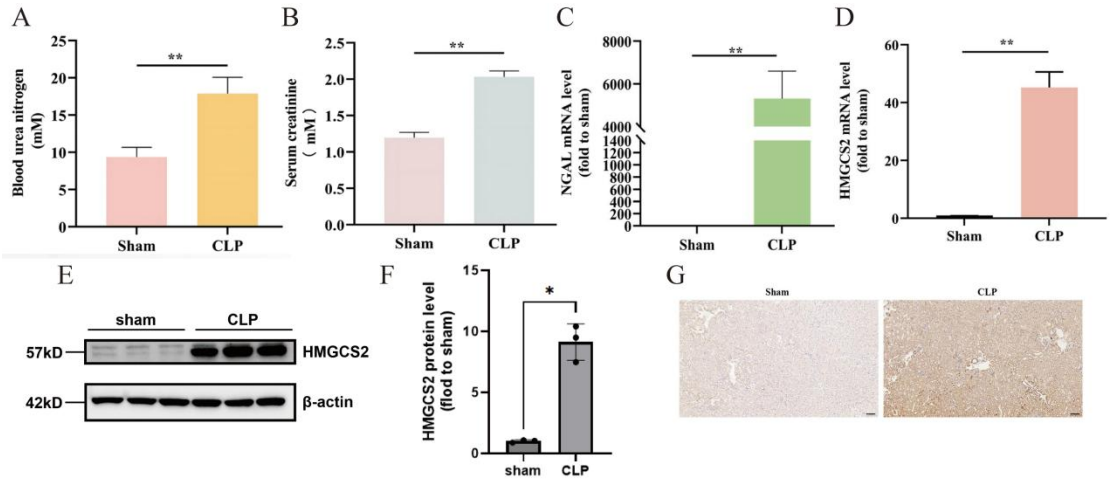


Figure 6 Upregulation of Hmgcs2 expression in the CLP-induced S-AKI mouse model

(A) Serum blood urea nitrogen (BUN) levels at 24 h after CLP surgery.

(B) Serum creatinine (Cr) levels at 24 h after CLP surgery.

(C) RT-qPCR detection of mRNA expression of the renal injury marker NGAL in mouse kidney tissues.

(D) RT-qPCR detection of Hmgcs2 mRNA expression in mouse kidney tissues.

(E) Representative Western blotting bands of HMGCS2 protein expression in mouse kidney tissues.

(F) Statistical graph of semi-quantitative analysis of relative HMGCS2 protein expression levels using ImageJ software.

(G) Immunohistochemistry (IHC) staining for HMGCS2 expression and localization in mouse kidney tissues (scale bar: 100 μm; brown indicates positive staining, blue indicates hematoxylin counterstaining of nuclei). Data are presented as mean ± standard deviation ($n \geq 3$); between-group comparisons were performed using two-tailed unpaired Student's t-test. $^{**}P < 0.01$.

Supplementary Files

This is a list of supplementary files associated with this preprint. Click to download.

- SupplementaryMaterial1018.docx